Journal of Materials Chemistry A

Accepted Manuscript

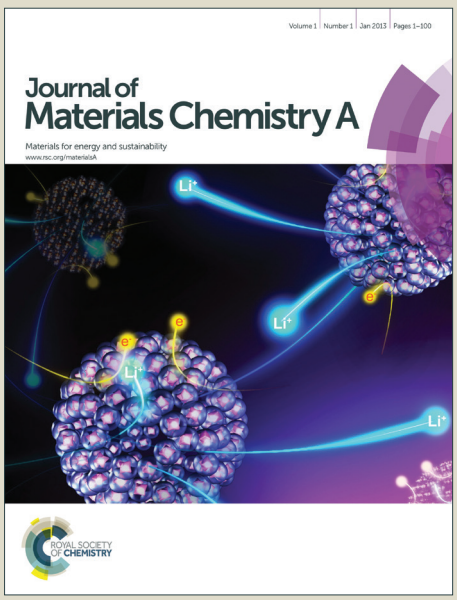

ROYAL SOCIETY OF CHEMISTRY

www.rsc.org/materialsA

Journal of Materials Chemistry A RSCPublishing

PAPER

Oxygen permeation and stability of Mo-substituted BSCF membranes

Cite this: DOI: 10.17638/datacat.liverpool.ac.uk/48

H. Gasparyan[a], J. B. Claridge[a] and M. J. Rosseinsky*[a]

Received 6th June 2015,
Accepted 22th June 2015

DOI: 10.17638/datacat.liverpool.ac.uk/48

www.rsc.org/

The oxygen permeation performance of $Ba_{0.5}Sr_{0.5}Co_{0.8-x}Fe_{0.2-y}Mo_{x+y}O_{3-\delta}$ (x+y=0; 0.025; 0.05; 0.25; 0.375 for Co/Fe=4 and x+y=0.125 for Co/Fe=2) ceramic perovskite materials was studied. The effects of the composition, structure, morphology and membrane thickness on permeation flux were investigated. We demonstrate how Mo substitution significantly improves the stability of BSCF membranes not only under static but also dynamic conditions by depressing the degradation rates at 750 °C. The highest permeation flux among the studied membranes was measured for a 1 mm thick $Ba_{0.5}Sr_{0.5}Co_{0.78}Fe_{0.195}Mo_{0.025}O_{3-\delta}$ as 1.55 ml min^{-1} cm^{-2} at 950 °C which is very close to the flux measured for BSCF (1.65 ml min^{-1} cm^{-2}) under the same conditions.

1. Introduction

Dense ceramic membranes exhibiting high mixed (oxygen) ionic and electronic conductivity (MIEC) have received attention as a potentially economic, clean and efficient way of producing oxygen by separation from air or other oxygen containing gas mixtures.[1, 2] High oxygen fluxes have been reported for mixed-conducting oxides with the perovskite structure.[3, 4] For example MIEC membranes of the $A_{1-x}Sr_xCo_{1-y}Fe_yO_{3-\delta}$ (A=La, Ba) perovskite oxides have been intensively studied by a number of research groups for oxygen separation[5-8] and partial oxidation of methane (POM).[9, 10] The main problem with these materials, that inhibits commercialization, is their structural instability[11-13] and high thermal expansion coefficients (TEC),[14-16] leading to formation of reduced phases under reducing conditions and hexagonal phases in oxygen rich atmospheres at intermediate temperatures (600-850 °C). Several research groups attempted to stabilize the cubic perovskite structure of $Ba_{0.5}Sr_{0.5}Co_{0.8}Fe_{0.2}O_{3-\delta}$ (BSCF) by substitution of less reducible metal ions on the B site[17-20], or by complete replacement of Co by Fe.[10, 21] We have shown previously that B site substitution of BSCF by Mo^{6+}, with similar ionic radius to Fe^{4+} and Co^{3+} but a higher charge, stabilizes the cubic structure at intermediate temperatures and enhances the electrochemical properties of BSCF as a cathode material.[22] The enhancements in properties are associated with the endotaxial intergrowth of Mo-rich double (DP) and Fe-rich single (SP) perovskite phases. In the present study we investigate the effect of partial substitution of B site cations by Mo on phase stability, oxygen permeability, thermal expansion and morphology as a function of temperature and time under the dynamic conditions of oxygen separation. Studies of the effect of membrane thickness on oxygen permeation flux and activation energy were also conducted.

2. Experimental section

2.1 Powder synthesis and characterization

A series of Mo-substituted BSCF ceramics with general formula $Ba_{0.5}Sr_{0.5}Co_{0.8-x}Fe_{0.2-y}Mo_{x+y}O_{3-\delta}$ (x+y=0; 0.025; 0.05; 0.25; 0.375 for Co/Fe=4 and x+y=0.125 for Co/Fe=2) have been synthesized via conventional solid state reaction. Stoichiometric amounts of $BaCO_3$ (99.997 %), $SrCO_3$ (99.994 %), Co_2O_3 (99.9985 %), Fe_2O_3 (99.998 %) and MoO_3 (99.998 %) all purchased from Alfa Aesar were hand ground in a pestle and mortar with the aid of acetone. Mixed precursors were then heated to 900 °C for 8 h with an intermediate step at 700 °C for 6 h. Fired powders were then ball milled (Fritsch Pulverisette 7) in isopropanol with ZrO_2 balls for approximately 22 h and pressed into pellets before firing at 1000 °C for 10 h. This step was repeated 4 times.

All materials were analyzed by XRD before and after the oxygen permeation measurements using a Panalytical X-ray diffractometer with Co $K\alpha_1$ monochromated radiation source (λ=1.789 Å) in the 5-80° 2θ range. Synchrotron X-ray diffraction data were obtained on beamline I11 at Diamond Light Source, UK, over $2 \leq 2\theta/^{o} \leq 90$ (λ= 0.827127 Å) at room temperature. The morphology of the membranes was characterized using scanning electron microscopy (Hitachi S-4800 Field-Emission Scanning Electron Microscope). TEC measurements were carried out in a NETZSCH DIL402C dilatometer in air over the 25-1000 °C temperature range.

Determination of oxygen content in series of $Ba_{0.5}Sr_{0.5}Co_{0.8-x}Fe_{0.2-y}Mo_{x+y}O_{3-\delta}$ powders were performed by iodometric titrations. Approximately 50 mg of powder was dissolved in 20 ml of 3 M hydrochloric acid (HCl) with an excess of potassium iodide (KI). The solution was then titrated with 0.1 M sodium thiosulphate ($Na_2S_2O_3$). $Na_2S_2O_3$ was standardized by titration against potassium iodate (KIO_3) dissolved in distilled water with KI and 1 M sulphuric acid.

2.2 Membrane fabrication and testing

The synthesized powders were pressed into disk shape at 4 tonnes using a 20 mm pellet die and then isostatically pressed at 200 MPa. These disks were sintered at 1140 °C for 5 h to achieve >96 % density. The density of the fabricated membrane was determined by the Archimedes method. Before oxygen permeation measurements pellets were polished to 1 mm (±0.05 mm) thickness using a Tegramin-30 polishing machine (Struers™) and SiC foils of 800-2000 grits.

The permeability of perovskite membranes under an oxygen partial pressure gradient were investigated in the Probostat™ (NorECs, Norway) measurement cell. Membrane pellets were sealed using gold gaskets by heating at 1057 °C for 8-10 h. 21 % oxygen balanced with nitrogen was used as the feed gas with a flow rate of 100 ml/min [STP], while 100 ml/min [STP] of He was used on the permeate side as a sweep gas. Oxygen permeation fluxes were measured using a Clarus 580 gas chromatograph (GC) equipped with a thermal conductivity detector (TCD). The pressure of sweep gas (He) was adjusted to 1 bar while the pressure of feed gas (air) was set to 1.4 bars to provide an O_2 partial pressure difference across the membrane. Initially the sweep side was purged with He to remove any air. Then N_2 gas was supplied into the feed side and the effluent of sweep gas, which consists of He and leaked N_2, was analyzed by the GC to assess the leakage. Permeation measurements were conducted only in the case when N_2 leakage was less than 5 % of the total permeation flux. Synthetic air (21 % O_2 balanced with N_2) was then supplied into the feed side and the permeated oxygen was measured. Oxygen permeation measurements were carried out upon decreasing temperature from 950 °C to 600 °C in 50 °C steps after stabilization for 15 minutes at each temperature. Oxygen permeation fluxes were calculated according to equation (1) assuming that leakage of N_2 and O_2 through cracks or pores is in accordance with the Knudsen diffusion mechanism (2):

$$J_{O_2}(mlcm^{-2}\ \min^{-1},[STP]) = [\frac{C_{O_2} - C_{N_2} \times 0.21}{0.79(28/32)^{1/2}}] \times \frac{F}{S} \quad (1)$$

$$\frac{J_{N_2}^{leak}}{J_{O_2}^{leak}} = \sqrt{\frac{32}{28}} \times \frac{0.79}{0.21} \quad (2)$$

Where,

C_{O_2}, C_{N_2} - measured concentrations of oxygen and nitrogen in the gas on the sweep side by GC (%)

F – Fixed flow rate of the sweep gas (100 ml/min)

S –Membrane surface area (~1.32 cm^2)

3. Results and discussions

3.1 Phase stability and thermal expansion

Fig. 1a shows room temperature X-ray diffraction patterns of $Ba_{0.5}Sr_{0.5}Co_{0.8-x}Fe_{0.2-y}Mo_{x+y}O_{3-\delta}$ membranes. As can be seen from the XRD patterns and calculated lattice parameters listed in Table 1, incorporation of Mo on the B site has a significant effect on the structure. Oxide powders with low Mo content (x+y = 0-0.125) have pure single cubic perovskite (SP) structures (space group $Pm\bar{3}m$, cell parameter $a_p \approx 3.9$ Å) with disordered substitution of Mo onto the octahedral B-site together with Co and Fe. With further increase of Mo substitution an additional diffraction peak with weaker intensity at 22.5° 2θ appears (Fig. 1b), which is attributed to the double perovskite (DP) structure (space group $Fm\bar{3}m$, cell parameter $2a_p \approx 7.9$Å) containing two distinct octahedral B-sites.

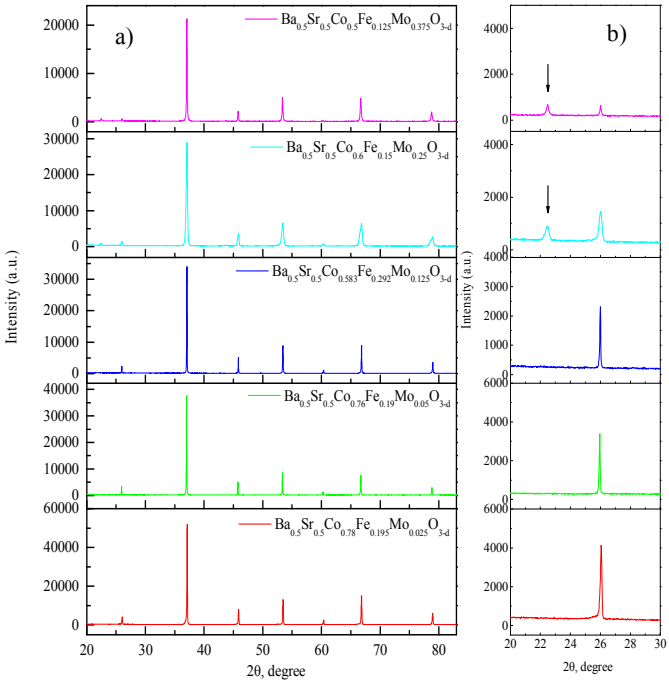

Fig.1: Room temperature XRD patterns of a) $Ba_{0.5}Sr_{0.5}Co_{0.8-x}Fe_{0.2-y}Mo_{x+y}O_{3-\delta}$ membranes sintered at 1140 °C for 5 h, b) zoomed section indicating double perovskite peaks at 2θ=22.5° (black arrows) for x+y=0.25 and 0.375 SP/DP compositions.

For the samples with x+y=0.25-0.375 the second perovskite phase coexists with the single perovskite as described and shown elsewhere.[22] As thermal stability tests in the air at 750 °C for 170 h were conducted for x+y=0.125, 0.25 and 0.375 powders previously[23] in this study we have performed similar aging tests at 750 °C for 170 h in air and flow of N_2 for the least Mo substituted BSCF composition (x+y=0.025). After these stability tests, powders were analyzed by synchrotron powder X-ray diffraction and are shown in the Fig. 2a and 2b. It has been extensively shown that instability of BSCF below 830 °C is caused by a reversible cubic to hexagonal phase transition driven by the reduction of B site Co^{4+}/Fe^{4+} cations into $Co^{3+/2+}/Fe^{3+}$.[24, 25] Further detailed investigation has revealed so-called plate-like or fishbone regions consisting of cubic, Fe depleted hexagonal and Co- and Ba-rich $Ba_{n+1}Co_nO_{3n+3}$ (n≥2) or BCO type crystal structures.[12] The presence of an additional monoclinic phase in BSCF after annealing at 750 °C for 10 h has also been reported.[26] However in the current study no significant changes or reflections corresponding to phases apart from the cubic perovskite were detected in XRD patterns of Mo substituted BSCF ceramic powders annealed in air or N_2 at 750 °C for 170 h (Fig. 2).

Several studies have reported high thermal expansion coefficient (TEC) values for Co containing MIEC materials and for BSCF in particular (~24-28E-6 K^{-1}).[14-16, 27] Table 1 summarizes TEC values of the $Ba_{0.5}Sr_{0.5}Co_{0.8-x}Fe_{0.2-y}Mo_{x+y}O_{3-\delta}$ ceramics in the 50-950 °C temperature range with the value for BSCF in good agreement with the literature.[14-16, 27] The observed sharp change in thermal expansion rate at temperatures of 400-500 °C have been reported by many researchers in BSCF-related materials.[14-16, 27] The phenomenon has been associated with the release of lattice oxygen to form oxygen

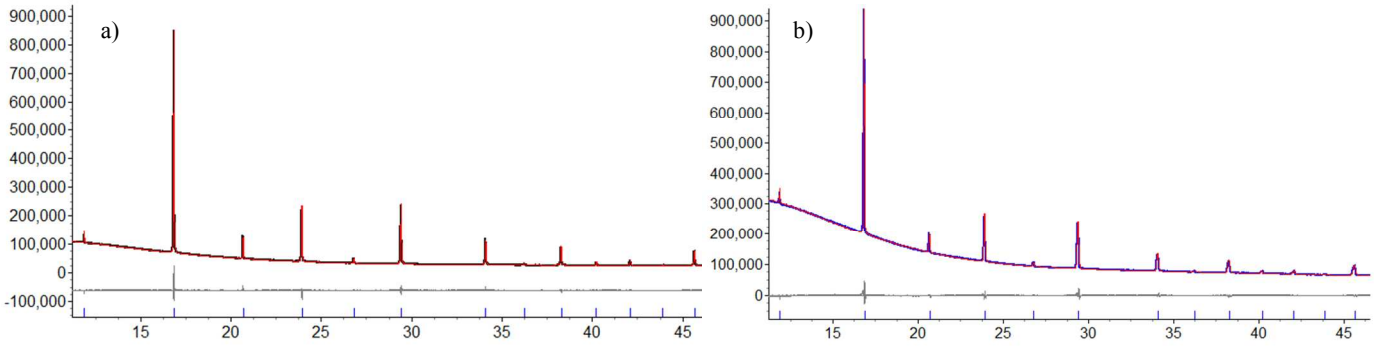

Fig.2: Observed (black/blue), calculated (red) and difference (grey) plots of Pawley refinements of room temperature synchrotron powder diffraction of the aged $Ba_{0.5}Sr_{0.5}Co_{0.78}Fe_{0.195}Mo_{0.025}O_{3-\delta}$ at 750 °C for 170 h a) in static air (a=3.9879(8) Å) and b) flowing nitrogen (a=3.9925(5) Å). Blue tick marks refer to SP.

vacancies, and reduction of Co and Fe, resulting in an increase of unit cell volume or chemical expansion.[28] In the low temperature region (LTR=50-500 °C) the thermal expansion coefficients of Mo-doped ceramics are very similar. In the high temperature region (HTR=550-950 °C) TECs decrease from 28.3×10^{-6} K^{-1} to 18.4×10^{-6} K^{-1} with increasing Mo content reaching the same values for both regions for $Ba_{0.5}Sr_{0.5}Co_{0.5}Fe_{0.125}Mo_{0.375}O_{3-\delta}$ (Table 1) which is an indication of enhanced thermal cycling stability.

Contradictory results have been reported in literature concerning the effect of the grain size on permeation flux of BSCF related materials. Zhang *et al.*[29] has reported that the oxygen permeation flux for a $SrCo_{0.8}Fe_{0.2}O_{3-\delta}$ membrane increased considerably with the decrease of the average grain size, indicating that the grain boundaries in the sample provided a faster path for oxygen diffusion and/or enhancement of the surface exchange rate.

Table 1: Summary of unit cell parameters calculated from Rietveld refinement and TEC values of $Ba_{0.5}Sr_{0.5}Co_{0.8-x}Fe_{0.2-y}Mo_{x+y}O_{3-\delta}$ ceramics.

Nominal composition	Lattice parameter SP/DP, Å	TEC, K^{-1} 50-500°C	TEC, K^{-1} 550-950°C
$Ba_{0.5}Sr_{0.5}Co_{0.8}Fe_{0.2}O_{3-\delta}$	3.9848(0)	11.2E-6	28.3E-6
$Ba_{0.5}Sr_{0.5}Co_{0.78}Fe_{0.195}Mo_{0.025}O_{3-\delta}$	3.9839(2)	17.8E-6	28.4E-6
$Ba_{0.5}Sr_{0.5}Co_{0.76}Fe_{0.19}Mo_{0.05}O_{3-\delta}$	3.9858(0)	17.5E-6	28.3E-6
$Ba_{0.5}Sr_{0.5}Co_{0.583}Fe_{0.292}Mo_{0.125}O_{3-\delta}$	3.9790(0)	17.9E-6	26.1E-6
$Ba_{0.5}Sr_{0.5}Co_{0.6}Fe_{0.15}Mo_{0.25}O_{3-\delta}$	3.9820(1) / 7.9927(3)	17.2E-6	22.1E-6
$Ba_{0.5}Sr_{0.5}Co_{0.5}Fe_{0.125}Mo_{0.375}O_{3-\delta}$	3.9899(1) / 7.9838(1)	18.6E-6	18.4E-6

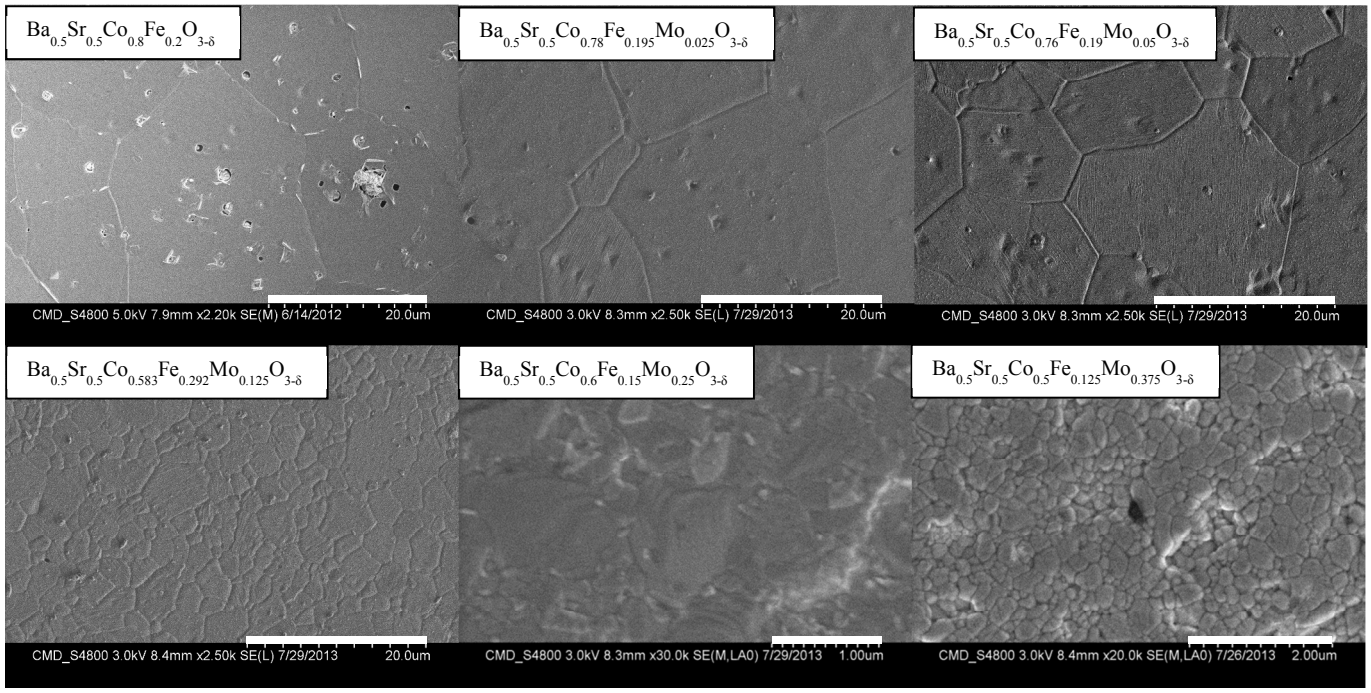

Fig. 3: SEM micrographs of the surface of $Ba_{0.5}Sr_{0.5}Co_{0.8-x}Fe_{0.2-y}Mo_{x+y}O_{3-\delta}$ membranes sintered at 1140 °C for 5h. Before SEM micrographs were taken all membranes were polished on both sides and thermally etched at 950 °C for 2 h for better grain boundary development.

Salehi *et al.*[30] and Baumann *et al.*[31] reported no significant difference in permeation flux performance for BSCF membranes sintered at different temperatures and with different grain sizes. Fig. 3 shows SEM images of $Ba_{0.5}Sr_{0.5}Co_{0.8-x}Fe_{0.2-y}Mo_{x+y}O_{3-\delta}$ membranes before permeation measurements. All 6 membranes after sintering at 1140 °C for 5 h were first polished and then thermally treated at 950 °C for 2 h in order to develop grain boundaries. As can be seen from the SEM images, all the pellets have a very dense structure. Increasing Mo content in the BSCF membrane leads to a significant decrease in the grain size changing from ~35 μm for

$Ba_{0.5}Sr_{0.5}Co_{0.78}Fe_{0.195}Mo_{0.025}O_{3-d}$ to 200-400 nm for $Ba_{0.5}Sr_{0.5}Co_{0.5}Fe_{0.125}Mo_{0.375}O_{3-\delta}$. A similar observation was reported for Al doped $SrFeO_{3-\delta}$.[32] It seems that grains of SP/DP structures in $Ba_{0.5}Sr_{0.5}Co_{0.6}Fe_{0.15}Mo_{0.25}O_{3-\delta}$ and $Ba_{0.5}Sr_{0.5}Co_{0.5}Fe_{0.125}Mo_{0.375}O_{3-\delta}$ membranes have not been fully sintered at 1140 °C as grain growth is not observed as in the case of the less substituted membranes. This indicates that increasing sintering temperature is required with increasing Mo doping. Attempts to sinter $Ba_{0.5}Sr_{0.5}Co_{0.6}Fe_{0.15}Mo_{0.25}O_{3-\delta}$ or $Ba_{0.5}Sr_{0.5}Co_{0.5}Fe_{0.125}Mo_{0.375}O_{3-\delta}$ at higher temperatures lead to impurity phase formation (XRD patterns are shown in the supplementary information S1 and S2).

3.2 Oxygen permeation measurements

The oxygen permeability of $Ba_{0.5}Sr_{0.5}Co_{0.8-x}Fe_{0.2-y}Mo_{x+y}O_{3-\delta}$ membranes with 1 mm thickness was examined in the temperature range of 600-950 °C and the results are shown in an Arrhenius-type plot (Fig. 4a). For comparison reasons 1 mm BSCF membrane was also tested under the same conditions. Increasing temperature results in increased oxygen permeation flux. It becomes clear that a lower Mo concentration, as in $Ba_{0.5}Sr_{0.5}Co_{0.78}Fe_{0.195}Mo_{0.025}O_{3-\delta}$, favours very high flux, ca. 1.55 ml min^{-1} cm^{-2} at 950 °C.

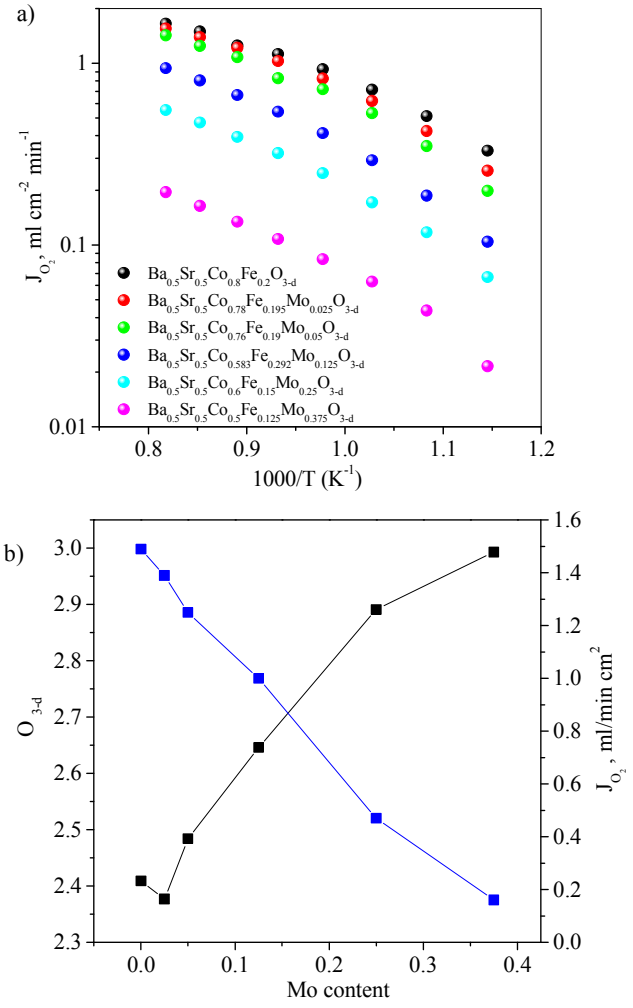

Fig. 4: Dependence of oxygen permeation flux J_{O2} on a) Mo doping level as a function of temperature (Arrhenius plot) and b) oxygen vacancy concentration.

Gradual reduction of oxygen permeation fluxes with increasing Mo substitution is expected and can be related to the reduction of the oxygen vacancy concentration measured by the iodometric titration technique (Fig. 4b). An increase in the oxygen content is required to compensate for increased charge on the B site as a result of substitution by Mo^{6+}, which is also expected to affect the material's ionic conductivity. Mauvy *et. al.*[33] have shown that permeability is proportional to the oxygen vacancy concentration and ionic conductivity, hence the observed decrease in oxygen permeability. The reduction of grain size caused by Mo substitution coupled with fewer oxygen vacancies does not favour a large permeation flux, which is consistent with the findings of Wang[27] and Niedrig[34] who have observed increase in oxygen flux and total conductivity with increasing grain size in BSCF membranes.

3.3 Rate determining steps

Oxygen transport through perovskite membranes can be controlled by the oxygen surface exchange kinetics, solid-state bulk diffusion or a combination of both. According to Wagner's theory [35] if the process is governed mainly by bulk diffusion, the oxygen permeation flux across the membrane is thickness dependent as shown in Eq. 3, where L is the thickness of the membrane.

$$j_{O_2} = \frac{RT}{4^2 F^2 L} \int_{P_{O2}^{lean}}^{P_{O2}^{rich}} \frac{\sigma_i \cdot \sigma_e}{(\sigma_i + \sigma_e)} \cdot d \ln P_{O_2} \qquad (3)$$

This means that, for process limited by bulk diffusion, upon reduction of the membrane's thickness the oxygen permeation flux should be enhanced. On the other hand, if the process is governed by surface exchange, the permeation flux should be thickness-independent, while the specific permeability (J_{O2} x L) will increase with increasing the membrane thickness. To clarify the controlling steps a systematic study was conducted on $Ba_{0.5}Sr_{0.5}Co_{0.78}Fe_{0.195}Mo_{0.025}O_{3-\delta}$ membranes of varying thickness L=1.6-0.75 mm. Oxygen permeation fluxes (J_{O2}) and specific permeability (J_{O2} x L) through these membranes, along with corresponding activation energies are presented in Fig. 5.

With increasing membranes thickness from 0.75 to 1.4 mm a pronounced decrease is observed in oxygen permeation fluxes above 750 °C (Fig. 5a), while below that temperature the change is not so significant. The increase in permeation flux with decreasing membrane's thickness indicates that the rate limiting step is the bulk diffusion. A change in rate limiting step and activation energy is observed on decreasing the temperature. In our studies the observed activation energies (inset of Fig. 5a) in the high temperature region (950-750 °C) are almost half those in the low temperature region (750-600 °C). At high temperature bulk diffusion is the most important contribution. On lowering the temperature surface exchange, involving adsorption/desorption, surface diffusion and charge transfer, becomes important due to its high activation energy[36]. However we do not reach the limiting case where surface exchange is the dominant rate determining step, as oxygen permeation flux would be independent of the thickness of the membrane. Our findings are consistent with results reported in the literature for BSCF. [36, 7, 14]

We have also found that with further increase in membrane thickness to 1.6 mm the permeation flux became thickness independent, while the specific permeability increased (Fig. 5b), indicating that for the thick samples the surface exchange is the rate limiting step. In support to our findings similar conclusion have been presented by Zeng *et al.* [37] where it was shown that for the thick 1.2 mm BSCF membrane permeation flux is limited by slow surface exchange kinetics.

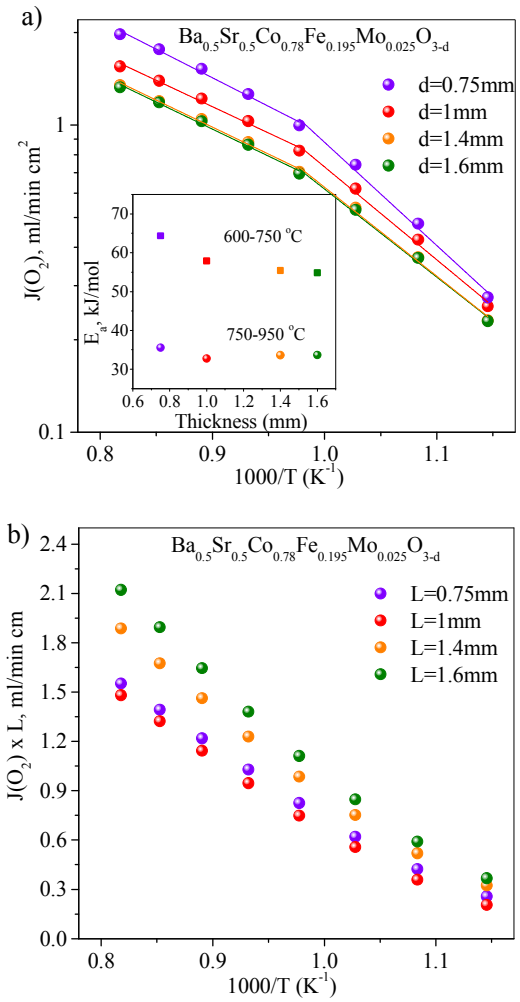

Fig. 5: The temperature dependence of a) permeation flux (J_{O2}) and b) specific permeability (J_{O2} x L) through the $Ba_{0.5}Sr_{0.5}Co_{0.78}Fe_{0.195}Mo_{0.025}O_{3-d}$ dense membrane with varying thickness (L=0.75-1.6 mm). The inset shows corresponding apparent activation energies of oxygen permeation as a function of membrane thickness.

3.4 Stability measurements under operating conditions

MIEC membranes should not only exhibit high oxygen permeation fluxes but also should be structurally stable under the operating conditions. In the section 3.1 we have demonstrated how Mo substitution improves BSCF thermal properties under static conditions. However the applied oxygen partial pressure gradient across the membrane during operation and the high permeation flux may influence the mobility of elements constituting the membrane due to the difference in self-diffusion coefficients causing kinetic demixing[38, 39] and jeopardising the stability of the material. An enrichment of the alkaline earth metals was found on the sweep side in $La_{0.3}Sr_{0.7}CoO_{3-\delta}$[40] and LSCF[41] membranes. Similar enrichment was also reported in the case of a BSCF membrane near the He inlet (sweep side) where $P(O_2)$ is relatively low.[38] Hence stability tests of the lowest and the highest Mo doped BSCF membranes, *i.e.*, $Ba_{0.5}Sr_{0.5}Co_{0.78}Fe_{0.195}Mo_{0.025}O_{3-\delta}$ (L=1.6mm) and $Ba_{0.5}Sr_{0.5}Co_{0.5}Fe_{0.125}Mo_{0.375}O_{3-\delta}$ (L=1mm), at 750 °C with air and He flow rates of 100 ml/min were conducted and are presented in Fig. 6. A stability test of a 1 mm BSCF membrane under the same conditions was also conducted for comparison.

As can be seen from Fig. 6, permeation fluxes of BSCF and $Ba_{0.5}Sr_{0.5}Co_{0.78}Fe_{0.195}Mo_{0.025}O_{3-\delta}$ membranes demonstrate two time-dependant decays which are absent in the case of the higher Mo doped membrane. The slopes obtained from linear fittings decrease by an order of magnitude for $Ba_{0.5}Sr_{0.5}Co_{0.78}Fe_{0.195}Mo_{0.025}O_{3-\delta}$ membrane (4.35×10^{-4} ml min^{-2} cm^{-2}) and 2 orders of magnitude for $Ba_{0.5}Sr_{0.5}Co_{0.5}Fe_{0.125}Mo_{0.375}O_{3-\delta}$ membrane (2.25×10^{-5} ml min^{-2} cm^{-2}) compared to BSCF (1.13×10^{-3} ml min^{-2} cm^{-2}).

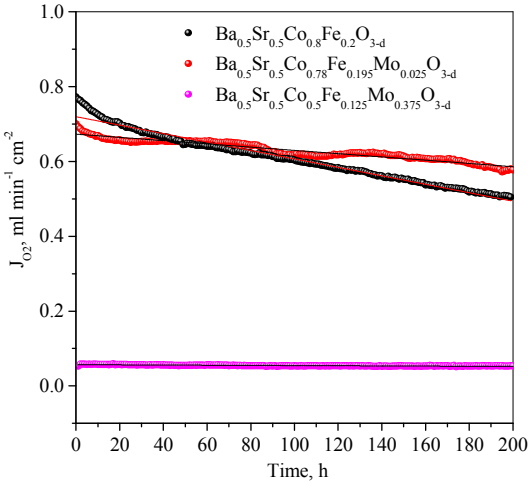

Fig. 6: Time dependence of oxygen permeation flux at 750 °C in 100/100 ml/min air/He for 1 mm BSCF, $Ba_{0.5}Sr_{0.5}Co_{0.78}Fe_{0.195}Mo_{0.025}O_{3-\delta}$ and $Ba_{0.5}Sr_{0.5}Co_{0.5}Fe_{0.125}Mo_{0.375}O_{3-\delta}$ membranes.

During 200 h of operation at 750 °C the BSCF membrane shows 35% decay of permeation flux, while $Ba_{0.5}Sr_{0.5}Co_{0.78}Fe_{0.195}Mo_{0.025}O_{3-\delta}$ demonstrates improved stability slowing the decay by a factor of two and resulting in only 17% reduction. We continuously measured the stability of $Ba_{0.5}Sr_{0.5}Co_{0.78}Fe_{0.195}Mo_{0.025}O_{3-\delta}$ membrane for additional 50 h and compared it with predicted value (from extrapolation of experimental data) of permeation flux for BSCF (results are shown in the supplementary information S3). After 250 h of operation permeation flux of $Ba_{0.5}Sr_{0.5}Co_{0.78}Fe_{0.195}Mo_{0.025}O_{3-\delta}$ membrane reduced to 19 %, while the predicted decay of BSCF membrane is over 43 %. This makes $Ba_{0.5}Sr_{0.5}Co_{0.78}Fe_{0.195}Mo_{0.025}O_{3-\delta}$ membrane superior to BSCF if considered for long term use at intermediate temperatures. On the other hand, the $Ba_{0.5}Sr_{0.5}Co_{0.5}Fe_{0.125}Mo_{0.375}O_{3-\delta}$ membrane from the beginning shows steady-state permeation. In the case of BSCF and $Ba_{0.5}Sr_{0.5}Co_{0.78}Fe_{0.195}Mo_{0.025}O_{3-\delta}$ the most rapid decay of permeation flux in the first 10 hs can be ascribed to the loss of the lattice oxygen.[8] According to Wang *et. al.*,[8] the estimated equilibrium time for a BSCF membrane (L=1.7 mm) at 875 °C is less than 10 min but can alter depending on the oxygen vacancy diffusion coefficient and the membrane thickness. The second and slower decay can be associated with formation of the Co_3O_4 and hexagonal phases. Most aging tests reported in the literature are conducted at higher temperatures[18, 20, 42] (above 830 °C) which makes the comparison problematic as permeation flux strongly depends on the experimental conditions such as the membrane thickness, temperature, oxygen partial pressure and gas flow rates on the sweep and the feed side.

Although XRD patterns and SEM images collected from the surfaces of all studied membranes have shown formation of Co_3O_4 and hexagonal phases on both sides (Fig 7b,7c and Fig. 8), decomposition products were detected only in the bulk of pure BSCF (Fig. 7a), but not in the bulk of Mo substituted membranes. Stability tests under static and dynamic conditions indicate that large differences in the oxygen partial pressure across the membrane may have a major influence on the membrane degradation, particularly

due to element mobility and interaction of migrating cations with gas species causing so-called kinetic demixing on the surface which was also observed for BSCF,[38] LSCF[41] and LSC[40] membranes.

SEM images of the aged membranes (Fig. 8) show how the feed sides of all membranes deteriorated to a greater extent that the sweep sides. However the feed side of the $Ba_{0.5}Sr_{0.5}Co_{0.78}Fe_{0.195}Mo_{0.025}O_{3-\delta}$ membrane seems less damaged compared to the feed side of the BSCF. Hexagonal and Co_3O_4 phases can clearly be seen growing in grains and at grain boundaries of BSCF and $Ba_{0.5}Sr_{0.5}Co_{0.78}Fe_{0.195}Mo_{0.025}O_{3-\delta}$ membranes (Fig. 8.1a and 8.2a).

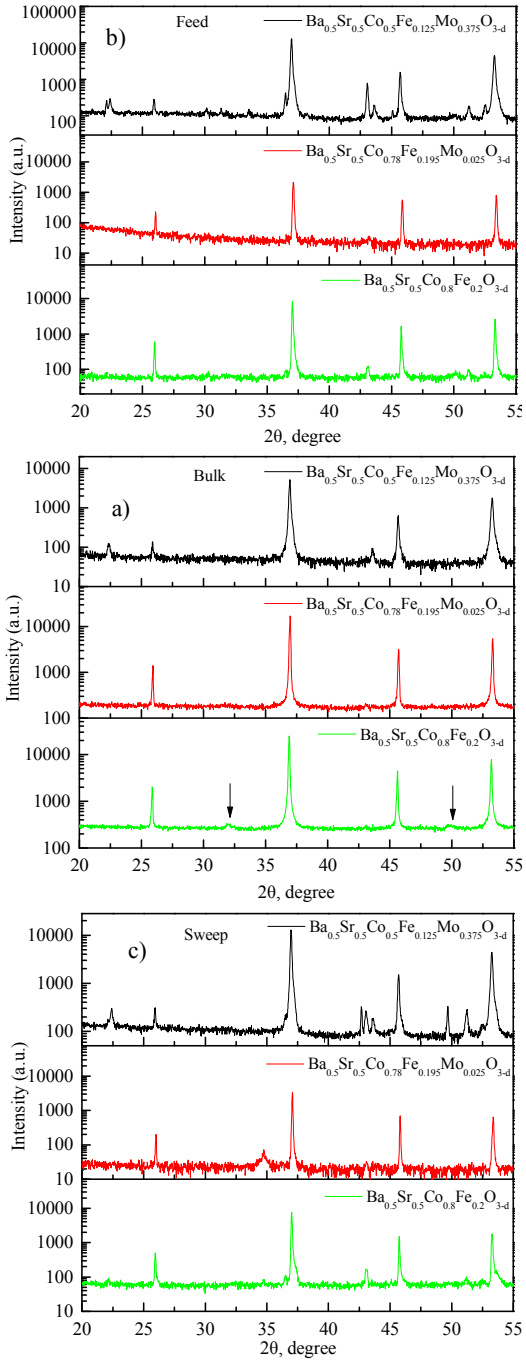

Fig. 7: XRD patterns (intensities presented in log scale) of BSCF, $Ba_{0.5}Sr_{0.5}Co_{0.78}Fe_{0.195}Mo_{0.025}O_{3-\delta}$ and $Ba_{0.5}Sr_{0.5}Co_{0.5}Fe_{0.125}Mo_{0.375}O_{3-\delta}$ membranes after aging at 750 °C for 200 h in 100/100 ml/min air/He: a) bulk of the membrane, b) feed and c) sweep sides. Arrowed peak indicate hexagonal phase.

SEM images of the $Ba_{0.5}Sr_{0.5}Co_{0.78}Fe_{0.195}Mo_{0.025}O_{3-\delta}$ membrane reveal significant grain growth in comparison with a fresh membrane. Although the hexagonal phase was detected by XRD on the surface of $Ba_{0.5}Sr_{0.5}Co_{0.5}Fe_{0.125}Mo_{0.375}O_{3-\delta}$ membrane, it was not observed by SEM imaging at grain boundaries. This may contribute to the stability at 750 °C over 200 h. The decomposition phases formed at the grain boundaries of the BSCF membrane reduce the permeation flux by 35 % after 200 h but do not affect the performance of the $Ba_{0.5}Sr_{0.5}Co_{0.5}Fe_{0.125}Mo_{0.375}O_{3-\delta}$ membrane. This indicates that grain boundaries have a critical effect on conductivity and permeability properties of BSCF. Decomposition of BSCF may not have such a strong effect on permeability if the secondary phases do not form along grain boundaries.

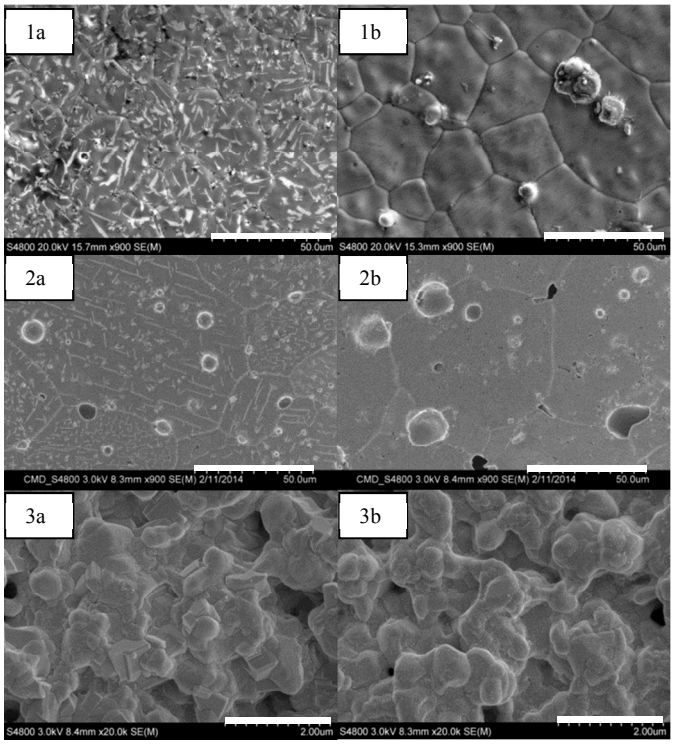

Fig. 8: SEM images of a) feed and b) sweep sides of 1) BSCF (L=1 mm), 2) $Ba_{0.5}Sr_{0.5}Co_{0.78}Fe_{0.195}Mo_{0.025}O_{3-\delta}$ (L=1.6 mm) and 3) $Ba_{0.5}Sr_{0.5}Co_{0.5}Fe_{0.125}Mo_{0.375}O_{3-\delta}$ (L=1 mm) membranes after stability tests at 750 °C for 200 h.

Conclusions

The $Ba_{0.5}Sr_{0.5}Co_{0.8-x}Fe_{0.2-y}Mo_{x+y}O_{3-\delta}$ ceramics have the single cubic perovskite structure at low Mo content and mixed single/double perovskite structure with higher Mo substitution levels. Stability tests in static oxidizing and reducing atmospheres have shown that doping BSCF with Mo significantly improves its stability. Gradual reduction of TEC values is observed with increasing Mo concentration in BSCF ceramics. The highest permeation flux of $J(O_2)$=1.55 ml min^{-1} cm^2 at 950 °C was measured for $Ba_{0.5}Sr_{0.5}Co_{0.78}Fe_{0.195}Mo_{0.025}O_{3-\delta}$ which is very close to the permeation flux of undoped BSCF $J(O_2)$=1.65 ml min^{-1} cm^2 at the same temperature. Permeation studies have shown that for 0.75-1.4 mm thick membranes the permeation flux is governed predominately by the bulk diffusion, however reducing the operating temperature increases the significance of surface exchange steps. The surface exchange is the rate-limiting step in relatively thick 1.6 mm membrane. We have demonstrated that partial decomposition of Mo substituted membranes takes place only on the surface of the

membrane and under large oxygen partial pressure differences across the membrane over a long period of time. These secondary phases do not affect the stable operation of the higher Mo doped membrane as they do not accumulate at grain boundaries.

Acknowledgements

We thank UK EPSRC (EP/H000925/1) and the STFC for access to Diamond, where we thank Dr. C. Tang and Dr. S. Thompson for assistance on the I11 diffractometer.

Notes and references

[a] Department of Chemistry, University of Liverpool, Liverpool L69 7ZD, United Kingdom.

*corresponding author: rossein@liv.ac.uk

Electronic Supplementary Information (ESI) available: [XRD patterns of the $Ba_{0.5}Sr_{0.5}Co_{0.5}Fe_{0.125}Mo_{0.375}O_{3-\delta}$ membrane sintered at 1200 ^{o}C and 1250 ^{o}C]. See DOI: 10.17638/datacat.liverpool.ac.uk/48

1. H. J. M. Bouwmeester and A. J. Burggraaf, in *Membrane Science and Technology*, eds. A. J. Burggraaf and L. Cot, Elsevier, Editon edn., 1996, vol. Volume 4, pp. 435-528.
2. H. Kruidhof, H. J. M. Bouwmeester, R. H. E. v. Doorn and A. J. Burggraaf, *Solid State Ionics*, 1993, **63–65**, 816-822.
3. P. Haworth, S. Smart, J. Glasscock and J. C. Diniz da Costa, *Sep. Purif. Technol.*, 2011, **81**, 88-93.
4. A. Thursfield and I. S. Metcalfe, *J. Mater. Chem.*, 2004, **14**, 2475-2485.
5. J. Sunarso, S. Baumann, J. M. Serra, W. A. Meulenberg, S. Liu, Y. S. Lin and J. C. Diniz da Costa, *J. Membr. Sci.*, 2008, **320**, 13-41.
6. D. Gao, J. Zhao, W. Zhou, R. Ran and Z. Shao, *J. Membr. Sci.*, 2011, **366**, 203-211.
7. S. Baumann, J. M. Serra, M. P. Lobera, S. Escolástico, F. Schulze-Küppers and W. A. Meulenberg, *J. Membr. Sci.*, 2011, **377**, 198-205.
8. H. Wang, Y. Cong and W. Yang, *J. Membr. Sci.*, 2002, **210**, 259-271.
9. H. Dong, Z. Shao, G. Xiong, J. Tong, S. Sheng and W. Yang, *Catal. Today*, 2001, **67**, 3-13.
10. H. Wang, C. Tablet, A. Feldhoff and J. Caro, *Adv. Mater.*, 2005, **17**, 1785-1788.
11. P. Müller, H. Störmer, L. Dieterle, C. Niedrig, E. Ivers-Tiffée and D. Gerthsen, *Solid State Ionics*, 2012, **206**, 57-66.
12. P. Müller, H. Störmer, M. Meffert, L. Dieterle, C. Niedrig, S. F. Wagner, E. Ivers-Tiffée and D. Gerthsen, *Chem. Mater.*, 2013, **25**, 564-573.
13. B. Wang, B. Zydorczak, D. Poulidi, I. S. Metcalfe and K. Li, *J. Membr. Sci.*, 2011, **369**, 526-535.
14. W. K. Hong and G. M. Choi, *J. Membr. Sci.*, 2010, **346**, 353-360.
15. C. Y. Park, T. H. Lee, S. E. Dorris, J. H. Park and U. Balachandran, *J. Power Sources*, 2012, **214**, 337-343.
16. S. McIntosh, J. Vente, W. Haije, D. H. A. Blank and H. Bouwmeester, *Chem. Mater.*, 2006, **18**, 2187-2193.
17. P. Shen, X. Liu, H. Wang and W. Ding, *J. Phys. Chem.C*, 2010, **114**, 22338-22345.
18. S. M. Fang, C. Y. Yoo and H. J. M. Bouwmeester, *Solid State Ionics*, 2011, **195**, 1-6.
19. Z. Wang, Y. Kathiraser and S. Kawi, *J. Membr. Sci.*, 2013, **431**, 180-186.
20. X. Chen, H. Liu, Y. Wei, J. Caro and H. Wang, *J. Alloys Compd.*, 2009, **484**, 386-389.
21. K. Efimov, T. Halfer, A. Kuhn, P. Heitjans, J. Caro and A. Feldhoff, *Chem. Mater.*, 2010, **22**, 1540-1544.
22. A. Demont, R. Sayers, M. A. Tsiamtsouri, S. Romani, P. A. Chater, H. Niu, C. Martí-Gastaldo, Z. Xu, Z. Deng, Y. Bréard, M. F. Thomas, J. B. Claridge and M. J. Rosseinsky, *J. Am. Chem. Soc.*, 2013, **135**, 10114-10123.
23. M. Tsiamtsouri, Doctoral thesis, University of Liverpool, 2012.
24. L. Ge, W. Zhou, R. Ran, S. Liu, Z. Shao, W. Jin and N. Xu, *J. Membr. Sci.*, 2007, **306**, 318-328.
25. S. Švarcová, K. Wiik, J. Tolchard, H. J. M. Bouwmeester and T. Grande, *Solid State Ionics*, 2008, **178**, 1787-1791.
26. M. Arnold, T. M. Gesing, J. Martynczuk and A. Feldhoff, *Chem. Mater.*, 2008, **20**, 5851-5858.
27. H. Wang, C. Tablet, A. Feldhoff and J. Caro, *J. Membr. Sci.*, 2005, **262**, 20-26.
28. J. Ovenstone, J.-I. Jung, J. S. White, D. D. Edwards and S. T. Misture, *J. Solid State Chem.*, 2008, **181**, 576-586.
29. K. Zhang, Y. L. Yang, D. Ponnusamy, A. J. Jacobson and K. Salama, *J. Mater. Sci.*, 1999, **34**, 1367-1372.
30. M. Salehi, F. Clemens, E. M. Pfaff, S. Diethelm, C. Leach, T. Graule and B. Grobéty, *J. Membr. Sci.*, 2011, **382**, 186-193.
31. S. Baumann, F. Schulze-Küppers, S. Roitsch, M. Betz, M. Zwick, E. M. Pfaff, W. A. Meulenberg, J. Mayer and D. Stöver, *J. Membr. Sci.*, 2010, **359**, 102-109.
32. V. V. Kharton, A. L. Shaula, F. M. M. Snijkers, J. F. C. Cooymans, J. J. Luyten, A. A. Yaremchenko, A. A. Valente, E. V. Tsipis, J. R. Frade, F. M. B. Marques and J. Rocha, *J. Membr. Sci.*, 2005, **252**, 215-225.
33. F. Mauvy, E. Boehm, J. M. Bassat, J. C. Grenier and J. Fouletier, *Solid State Ionics*, 2007, **178**, 1200-1204.
34. C. Niedrig, S. Taufall, M. Burriel, W. Menesklou, S. F. Wagner, S. Baumann and E. Ivers-Tiffée, *Solid State Ionics*, 2011, **197**, 25-31.
35. C. Wagner, *Prog. Solid State Chem.*, 1975, **10, Part 1**, 3-16.
36. Z. Shao and S. M. Haile, *Nature*, 2004, **431**, 170-173.
37. P. Zeng, Z. Chen, W. Zhou, H. Gu, Z. Shao and S. Liu, *J. Membr. Sci.*, 2007, **291**, 148-156.
38. J. Vente, S. McIntosh, W. Haije and H. Bouwmeester, *J. Solid State Electrochem.*, 2006, **10**, 581-588.
39. J.-I. Jung and D. D. Edwards, *J. Eur. Ceram. Soc.*, 2012, **32**, 3733-3743.
40. R. H. E. van Doorn, H. J. M. Bouwmeester and A. J. Burggraaf, *Solid State Ionics*, 1998, **111**, 263-272.
41. M. M. Viitanen, R. G. v. Welzenis, H. H. Brongersma and F. P. F. van Berkel, *Solid State Ionics*, 2002, **150**, 223-228.
42. X. Zhu, H. Wang and W. Yang, *Solid State Ionics*, 2006, **177**, 2917-2921.